

EVOLUTION OF DUST IN PRIMORDIAL SUPERNOVA REMNANTS: CAN DUST GRAINS FORMED IN THE EJECTA SURVIVE AND BE INJECTED INTO THE EARLY INTERSTELLAR MEDIUM?

TAKAYA NOZAWA,¹ TAKASHI KOZASA,¹ ASAO HABE,¹ ELI DWEK,² HIDEYUKI
UMEDA,³ NOZOMU TOMINAGA³, KEIICHI MAEDA⁴ and KEN'ICHI NOMOTO^{3,5}

ABSTRACT

We investigate the evolution of dust that formed at Population III supernova (SN) explosions and its processing through the collisions with the reverse shocks resulting from the interaction of the SN ejecta with the ambient medium. In particular, we investigate the transport of the shocked dust within the SN remnant (SNR), and its effect on the chemical composition, the size distribution, and the total mass of dust surviving in SNR. We find that the evolution of the reverse shock, and hence its effect on the processing of the dust depends on the thickness of the envelope retained by the progenitor star. Furthermore, the transport and survival of the dust grains depend on their initial radius, a_{ini} , and composition: For Type II SNRs expanding into the interstellar medium (ISM) with a density of $n_{\text{H},0} = 1 \text{ cm}^{-3}$, small grains with $a_{\text{ini}} \lesssim 0.05 \mu\text{m}$ are completely destroyed by sputtering in the postshock flow, while grains with $a_{\text{ini}} = 0.05\text{--}0.2 \mu\text{m}$ are trapped into the dense shell behind the forward shock. Very large grains of $a_{\text{ini}} \gtrsim 0.2 \mu\text{m}$ are ejected into the ISM without decreasing their sizes significantly. We find that the total mass fraction of dust that is destroyed by the reverse shock ranges

¹Department of CosmoSciences, Graduate School of Science, Hokkaido University, Sapporo 060-0810, Japan; tnozawa@mail.sci.hokudai.ac.jp

²Laboratory for Astronomy and Solar Physics, NASA Goddard Space Flight Center, Greenbelt, MD 20771

³Department of Astronomy, School of Science, University of Tokyo, Bunkyo-ku, Tokyo 113-0033, Japan

⁴Max-Planck-Institut für Astrophysik, Karl-Schwarzschild Strasse 1, 85741 Garching, Germany

⁵Research Center for the Early Universe, School of Science, University of Tokyo, Bunkyo-ku, Tokyo 113-0033, Japan

from 0.2 to 1.0, depending on the energy of the explosion and the density of the ambient ISM. The results of our calculations have significant impact on the abundance pattern of subsequent generation of stars that form in the dense shell of primordial SNRs.

Subject headings: dust, extinction — early universe — shock waves — supernova remnants — supernovae: general

1. INTRODUCTION

Recent far-infrared to millimeter observations of quasars with redshifts $\gtrsim 5$ have revealed the presence of large amount of dust with masses in excess of $10^8 M_\odot$ (Bertoldi et al. 2003; Priddey et al. 2003; Robson et al. 2004; Beelen et al. 2006). The presence of these large quantities of dust at such early epoch when the universe was $\lesssim 1$ Gyr old, suggests the rapid enrichment with dust that formed in the explosive ejecta of short-lived massive stars (Morgan & Edmunds 2003, Maiolino et al. 2004b; Dwek et al. 2007). In addition, Maiolino et al. (2004a) have reported that the dust extinction curve of the broad absorption line quasar SDSS1048+46 at $z = 6.2$ is quite different than those of quasars at $z < 4$, suggesting different dust sources and evolutionary histories.

Dust plays a pivotal role in the interstellar processes that determine the state of the interstellar medium (ISM). Dust affects the thermal and chemical balance of the ISM by reprocessing the radiative outputs from stars, providing photoelectrons that heat the gas, and depleting the gas of refractory elements that are important cooling agents of the ISM. Dust also serves as a catalyst for chemical reactions, especially the formation of H_2 molecules on the surface of dust grains (Hirashita & Ferrara 2002; Cazaux & Spaans 2004). In addition, the cooling of gas through thermal radiation from dust triggers the fragmentation of star-forming cloud into low-mass gas clumps of $\sim 0.1\text{--}1 M_\odot$ even for the metallicity of $10^{-6}\text{--}10^{-5} Z_\odot$ (Omukai et al. 2005; Schneider et al. 2006), although very massive stars of $\gtrsim 100 M_\odot$ are considered to be formed up to $Z \simeq 10^{-3.5} Z_\odot$ without the effect of dust (Bromm et al. 2001). Finally, dust obscures the nature of underlying stellar populations (e.g., Hines et al. 2006) and physical processes in the early universe. Understanding the origin and the complex evolutionary history of dust is therefore one of the most important goals in astrophysics.

During the first Gyr of cosmic history, supernovae (SNe) are the only possible source of interstellar dust, since low mass stars have not had time to evolve off the main sequence and inject the dust that forms in their quiescent outflows into the ISM. Theoretical studies aimed at determining the composition and yield of dust in the ejecta of primordial Type II

SNe (SNe II) and pair-instability SNe (PISNe) were conducted by Todini & Ferrara (2001), Nozawa et al. (2003), and Schneider et al. (2004). These works have shown that even the first SNe evolving from zero-metal progenitor stars can efficiently produce dust at 150–800 days after the explosion. The ratio of the total dust mass to the progenitor mass M_{pr} is 0.02–0.05 for SNe II with $M_{\text{pr}} = 12\text{--}35 M_{\odot}$ and 0.15–0.3 for PISNe with $M_{\text{pr}} = 140\text{--}260 M_{\odot}$. The composition of the newly formed dust grains are controlled by the elemental composition inside the He core, and their sizes range from 0.001 μm to 1 μm , depending on the concentration of the gas species forming dust and the time evolution of temperature and density of gas.

The results of these calculations have been applied to study the high-redshift dust. Maiolino et al. (2004b) demonstrated a SN origin for high-redshift dust, showing that the extinction curve of the $z = 6.2$ quasar SDSS1048+46 can be nicely fitted by the SN II dust models from Todini & Ferrara (2001). Dust produced in the unmixed SNe II by Nozawa et al. (2003) can also successfully reproduce the extinction curve of the quasar SDSS1048+46 by weighting the progenitor mass with the Salpeter initial mass function (Hirashita et al. 2005). Adopting the dust models by Nozawa et al. (2003), Nozawa et al. (2006) investigated the destruction of dust in the early ISM by the high-velocity shocks driven by SNe, and derived the timescale of dust destruction in the early universe as a function of the explosion energy of SNe and the gas density in the ISM. It should be pointed out here that these studies implicitly assumed that dust grains formed in SNe are injected into the ISM without their composition and size distribution being reprocessed.

However, the interaction of the SN ejecta with the surrounding medium will create a reverse shock which will process the grains that condensed in the He core before their injection into the ISM. Once the newly formed dust grains encounter the reverse shock, they acquire the high velocities relative to the gas and penetrate into the hot gas created by the passage of the reverse shock and forward shock. These dust grains are eroded by the kinetic sputtering and are also decelerated by the drag force of the gas. Small grains decelerate efficiently, and become trapped in the hot gas, where they are efficiently destroyed by thermal sputtering. On the other hand, large grains can maintain their high velocities, pass through the shocked gas and the outwardly expanding shock front, and be injected into the ISM without significant destruction. The net amount and composition of the dust that is eventually returned to the ISM by SNe differs substantially from the dust that was in the SN ejecta shortly after its formation.

In this paper, we study the evolution of dust formed in primordial SNe II and PISNe, considering its processing through the collisions with the reverse shocks and its transport within SNRs, based on the dust formation calculations by Nozawa et al. (2003). The

questions that we pose here are what fraction of dust grains formed in Population III SNe can survive the hostile circumstances within SNRs and how their size distributions can be altered by sputtering in the postshock flow. This subject has not been fully explored to date. Recently, Bianchi & Schneider (2007) have studied the evolution of newly condensed grains through the passage of the reverse shock by using a semi-analytical model and have showed that the fraction of dust mass survived ranges between 2 % and 20 % depending on the density in the ISM. However, they consider only the dust evolution in the nonradiative phase of SNR up to about $4\text{--}8 \times 10^4$ yr from the SN explosion, without taking into account the motion of dust relative to gas caused by the drag force which strongly affects the destruction process and evolution of dust in SNRs. In the calculations, we carefully treat the dynamics and destruction of dust and the time evolution of the temperature and density of the gas within SNRs until $\sim 10^5\text{--}10^6$ yr extending over a period of the radiative phase, in order to reveal how much amount of dust is finally injected into the ISM or destroyed completely. Although we focus on Population III SNe in this paper, this study can also give great insight into the evolution of dust in Galactic SNRs.

In § 2, we describe the initial conditions for the evolution of SNRs, the model of dust inside the He core, and the physics of dust and gas within SNRs. In § 3, we present and discuss the results of calculations. In § 4, we shall discuss the effects of the hydrogen envelope on the evolution of dust in SNRs. As an application of the result, we investigate the abundance patterns of the second-generation stars formed in the dense shell of Population III SNRs in § 5. The summary is presented in § 6.

2. THE MODEL OF CALCULATIONS

2.1. *The Initial Conditions for the Evolution of SNRs*

The evolution of SNR is described by three characteristic parameters; explosion energy, ejecta mass, and the density profile of the ambient gas (Truelove & McKee 1999). In this paper, we focus on the evolution of ejecta expanding into a uniform ambient medium whose elemental composition is primordial. To investigate the dependence of the efficiency of dust destruction on the ambient gas density, we consider three cases for the hydrogen number density in the ISM; $n_{\text{H},0} = 0.1, 1, \text{ and } 10 \text{ cm}^{-3}$. The temperature of gas T_0 in the ISM can be also affect the evolution of SNRs, since the ambient pressure regulates the deceleration of blast wave. However, we have confirmed that the results of calculations are almost independent of the value of T_0 , provided that $T_0 = 10^3\text{--}10^5$ K. Thus, we assume here $T_0 = 10^4$ K regardless of the gas density in the ISM, referring to the studies showing that the radiative feedback from the massive pre-SN stars can cause the ambient ISM to heat up to $T_0 \sim 10^4$

K (Kitayama et al. 2004; Machida et al. 2005).

The initial conditions for the structures of density and velocity in the ejecta are taken from the hydrodynamic models of Population III SNe by Umeda & Nomoto (2002). We adopt six SN models; four SNe II and two PISNe. The explosion energy of SNe II with $M_{\text{pr}} = 13, 20, 25,$ and $30 M_{\odot}$ is 10^{51} erg, and that of PISNe with $M_{\text{pr}} = 170$ and $200 M_{\odot}$ is 2×10^{52} erg and 2.8×10^{52} erg, respectively. It should be mentioned here that the massive metal-free stars cannot lose significant mass during their lifetime due to pulsations and line-driven stellar winds which are considered to be important at high metallicities (Baraffe et al. 2001). Although Smith & Owocki (2006) have suggested that the mass loss of very massive stars above roughly $40\text{--}50 M_{\odot}$ may be possible by continuum-driven winds or hydrodynamic explosions being insensitive to metallicity, the mechanism to trigger such a mass loss is an open question. Thus, we consider that Population III PISNe as well as SNe II have retained their thick hydrogen envelopes at the time of explosion.

2.2. *Dust Model inside the He core*

In the ejecta of SNe, dust grains can nucleate and grow only in the metal-rich cooling gas, and their composition and size distribution largely depend on the elemental abundance inside the He core (Kozasa et al. 1989). Accordingly, Nozawa et al. (2003) have calculated the dust formation in Population III SNe by considering two cases for the elemental composition inside the He core. They found that in the unmixed ejecta with the original onion-like structure, a variety of grain species condense in each layer. The main grain species are C grain in carbon-rich He layer; Al_2O_3 , Mg_2SiO_4 , and MgO grains in O-Mg-Si layer; Al_2O_3 , MgSiO_3 , and SiO_2 grains in O-Si-Mg layer; Si and FeS grains in Si-S-Fe layer; Fe grain in the innermost Fe-Ni core. On the other hand, oxide (Al_2O_3 and Fe_3O_4) and silicate (MgSiO_3 , Mg_2SiO_4 , and SiO_2) grains are formed in the uniformly mixed ejecta with $\text{C}/\text{O} < 1$, where the efficiency of unity is assumed for the formation of CO and SiO molecules.

Dust grains inside the He core are never processed by kinetic or thermal sputtering before they hit the reverse shock, because they move with the same velocities as the gas, and the gas temperature within the He core is too low for dust grains to be destroyed by the thermal sputtering. Therefore, as the initial condition of dust residing within the He core, we adopt the size distribution, mass fraction, and spatial distribution of each dust species calculated by Nozawa et al. (2003). In what follows, we refer to the dust grains created in the unmixed and mixed ejecta as the unmixed grain model and the mixed grain model, respectively.

2.3. *Physics of Gas and Dust in SNRs*

The collision of the expanding SN ejecta with the surrounding ISM simultaneously creates a forward shock at the interface between the ejecta and the ISM, and a reverse shock that penetrates into the ejecta. Once the reverse shock encounters dust grains inside the He core, the dust grains are decoupled from the comoving gas to ballistically intrude into the hot gas heated by the reverse shock, and then they are eroded via the kinetic sputtering because of high velocities relative to gas. If dust grains are trapped into the postshock flow owing to the gas drag, they are destroyed via the thermal sputtering caused by the thermal motion of gas. These dust particles are also heated by the collisions with the gas and radiate the thermal emission to cool the postshock gas. The rates of deceleration, erosion by sputtering, and heating of dust grains depend on not only their chemical composition and size but also the temperature and density of the gas in the postshock flow.

Recently, Nozawa et al. (2006, NKH06) have calculated the dust destruction in the high-velocity interstellar shocks driven by SNe in the early universe, by carefully treating the dynamics, erosion, and heating of dust grains, taking account of their size distribution and the time evolution of the temperature and density of the gas in the postshock flow. The present calculations of the dust evolution within SNRs follow the method described in NKH06 (see, NKH06 for details). We briefly mention the outline, focusing on the difference in the cooling function used in the calculations.¹

We assume that the spherically symmetric ejecta collides with the ISM in 10 yr after the explosion. With the initial conditions described in § 2.1, the time evolution of the gas in SNRs is numerically solved with the flux-splitting method (van Albada, et al. 1982; Mair et al. 1988). In the calculations, we include three processes of the radiative cooling in the equation of the conservation of energy. The first is the thermal emission from dust collisionally heated in the postshock flow, and the second is the inverse Compton cooling, whose rate is calculated at the redshift of $z = 20$. The third is the cooling of gas by the

¹ Note that in the calculation we neglect the effect of Coulomb drag on the motion of dust: The ratio of the Coulomb drag force to the gas drag force is given by $\sim \phi^2 \ln \Lambda (G_{\text{plasma}}(s)/G_{\text{coll}}(s))$ (Draine & Salpeter 1979), where ϕ is the dimensionless potential parameter, Λ is the Coulomb cutoff factor, and s is defined by $s^2 = mw_d^2/2kT$ with m the mass of gas and w_d the velocity of dust relative to gas. $G_{\text{plasma}}/G_{\text{coll}} < 1$ for $0 < s < \infty$ (Draine & Salpeter 1979), $\ln \Lambda \sim 30\text{--}40$ in SNRs (Dwek & Arendt 1992), and ϕ is evaluated to be $\sim 10^5/T$ for the gas temperature of $T \gtrsim 10^{5.5}$ K (McKee et al. 1987). Thus, the Coulomb drag is negligible compared with the gas drag for $T \gtrsim 10^6$ K, otherwise it can play important role in the deceleration of dust. However, the erosion rate of dust grains by thermal sputtering quickly decreases at $T \lesssim 10^6$ K (NKH06). As a result, the Coulomb drag does not significantly affect the motion and destruction of dust grains considered in this paper.

atomic process. For the gas with the primordial composition in the hydrogen envelope and behind the forward shock, we adopt the atomic cooling function for the zero metal case given by Sutherland & Dopita (1993) that is limited to the gas temperature of $T \geq 10^4$ K. In order to calculate the evolution of the gas in the dense shell appeared at the later phase of SNRs, we extrapolate the cooling rate of gas at $T < 10^4$ K as follows. Referring to Machida et al. (2005), the atomic cooling rate at $T < 10^4$ K is approximately proportional to T^4 ; the cooling rate decreases from $\Lambda^{\text{gas}} \simeq 10^{-23}$ erg cm $^{-3}$ s $^{-1}$ at $T = 10^4$ K to $\Lambda^{\text{gas}} \simeq 10^{-27}$ erg cm $^{-3}$ s $^{-1}$ at $T = 10^3$ K. Therefore, we simply evaluate the atomic cooling rate as $\Lambda^{\text{gas}} = T_4^4 \Lambda_4^{\text{gas}}$, where T_4 is the gas temperature in units of 10^4 K and Λ_4^{gas} is the atomic cooling rate at $T = 10^4$ K. For the metal-rich He core, we assume that the gas is only composed of oxygen which is the most abundant gas species inside the He core, and employ the cooling functions from Smith et al. (2001) for $T \geq 10^5$ K and Raymond & Smith (1977) for $T < 10^5$ K. In the calculations, we ignore the contribution of cooling by metal ions released from dust by sputtering for simplicity.

The dynamics and destruction of dust after colliding with the reverse shocks are calculated as follows. By treating dust as a test particle and ignoring the effect of charge on dust grains, the deceleration rate of dust due to the gas drag is calculated for each size of the dust to evaluate the velocity relative to gas and the position. Then we calculate the dust destruction by sputtering and the heating by collisions with the gas, using the relative velocity and the temperature and density of gas at the position. The sputtering yield of each dust species is calculated with the universal relation derived by NKH06. Dust grains are considered to be completely destroyed when their sizes become smaller than the radius of the nominal monomer of condensate. The cooling of gas through thermal emission of dust is calculated by balancing the heating of dust resulting from the collisions with electrons. The calculations are performed by the truncation time at which the forward shock velocity decelerates below 20 km s $^{-1}$.

3. RESULTS

In this section, we present the results of the calculations of dust evolution within primordial SNRs. In § 3.1, we demonstrate the time evolution of temperature and density of gas in the SNR, and in § 3.2, we show the transport and destruction of dust grains within SNRs. In § 3.3, we provide the resulting size distribution of survived dust and elucidate the dependence of the efficiency of dust destruction on the progenitor mass and the gas density in the ISM.

3.1. Time Evolution of the Gas in the SNRs

Figure 1 shows the time evolution of the density (Fig. 1a) and temperature (Fig. 1b) of gas by 2×10^4 yr in the SNR generated from the explosion of star with $M_{\text{pr}} = 20 M_{\odot}$ and expanding into the ISM with $n_{\text{H},0} = 1 \text{ cm}^{-3}$. The unmixed grain model is taken as the model of dust inside the He core, and the cooling of gas by dust is taken into account. In what follows, we refer to this model as the standard model.

The forward shock resulting from the interaction of the ambient gas with the ejecta of the SN is specified by the steep rise of the gas temperature and the increase of the gas density by ~ 4 times that in the ISM. The downward arrows in Figure 1a show the positions of the forward shock. We can also identify the formation of the reverse shock from high temperature of gas heated by the compression of the ejecta, and indicate its position for each time by the downward arrow in Figure 1b.

The position R_{rs} (Fig. 2a) and velocity V_{rs} (Fig. 2b) of this reverse shock as a function of time are depicted by the thick solid curves in Figure 2. The reverse shock is decelerated by the shocked ambient medium while it initially expands outward, and then returns back at a distance of ~ 5 pc (1.5×10^{19} cm) with the velocity of a few 100 km s^{-1} . The trajectory of the reverse shock is affected by the detail structure of density in the ejecta. The collision with the locally high-density gas inside the He core causes the reverse shock to move outward again at 5200 yr. After 1.1×10^4 yr, the reverse shock goes inward through the He core with increasing its velocity up to $>1000 \text{ km s}^{-1}$. Hence, dust grains crossing the reverse shock acquire the different velocities relative to gas, depending on the time of collision with the reverse shock, and are efficiently eroded by the kinetic sputtering if the relative velocity is $\sim 500\text{--}1300 \text{ km s}^{-1}$.

It can be seen from Figure 1 that the temperature of the gas in the region between the forward and reverse shocks is higher than 10^6 K. Thus, dust grains staying in this region are subject to the thermal sputtering. However, the erosion rate of dust decreases as the SNR evolves because the density decreases with time. Around the truncation time ($\simeq 8 \times 10^5$ yr for the standard model), the gas density within the SNR is more than 100 times lower than that in the ISM, and the gas temperature becomes low (\sim several times 10^5 K) enough for dust grains not to be sputtered efficiently, and thus the destruction of dust via the sputtering is extremely inefficient.

The influence of the cooling by dust on the SNR evolution is clarified by comparing the results of calculations with and without the cooling by dust emission. The evolution of the reverse shock without the dust cooling for $M_{\text{pr}} = 20 M_{\odot}$ and $n_{\text{H},0} = 1 \text{ cm}^{-3}$ is shown by the thick dashed curves in Figure 2, where the cooling of gas by dust can cause the velocity of

the reverse shock to be reduced by $\sim 10\%$. The thin curves in Figure 2 show the evolution of the reverse shock penetrating into the ejecta of PISN with $M_{\text{pr}} = 170 M_{\odot}$ calculated for $n_{\text{H},0} = 1 \text{ cm}^{-3}$. Because the thermal emission from dust increases with increasing the dust mass, the effects of cooling by dust are significant for the remnants of PISNe, where the mass of dust formed in the ejecta is a few tens M_{\odot} . As we can see from the figure, the velocity of the reverse shock including dust cooling (*thin solid line*) decreases to 0.6 times that not including the cooling (*thin dashed line*) at $\gtrsim 7000$ yr. In addition, the dust cooling decreases the gas temperature by $\sim 20\%$, compared with that calculated without dust cooling. However, it should be noted that the efficiency of dust destruction is little affected by the dust cooling, because most of dust grains are predominantly destroyed by the thermal sputtering and the erosion rate is not sensitive to the gas temperature as long as $T > 10^6$ K (NKH06). Note that the cooling by oxygen line has no influence on the results, since the temperature within the He core during the passage of the reverse shock is above 10^7 K where the dominant cooling process of gas is free-free emission.

3.2. *Transport and Destruction of Dust in SNR*

The time evolutions of the positions (Fig. 3a) and sizes (Fig. 3b) of dust grains within the SNR for the standard model are given in Figure 3. In Figure 3a, the trajectories of the forward and reverse shocks are also depicted by the thick solid curves, along with the position of the surface of the He core. Among nine dust species in the unmixed grain model, are shown C, Mg_2SiO_4 , and Fe grains with the initial sizes of $0.01 \mu\text{m}$ (*dotted lines*), $0.1 \mu\text{m}$ (*solid lines*), and $1 \mu\text{m}$ (*dashed lines*), respectively. Each grain species initially moves coupling with the gas with the velocity of ~ 1300 , ~ 900 , and $\sim 400 \text{ km s}^{-1}$ for C, Mg_2SiO_4 , and Fe grains, respectively, and collides with the reverse shock at 3650 yr for C grains formed in the outermost He core, 6300 yr for Mg_2SiO_4 grains in the oxygen-rich layer, and 13000 yr for Fe grains condensed in the innermost He core.

The collision time of the reverse shocks with dust grains depends on the initial velocity and position of dust, the thickness of the hydrogen envelope, and the density in the ISM. Figure 4 gives the collision time t_{coll} of the reverse shock with the He core for different progenitor mass and gas density in the ISM. We can see that the collision time is shorter for PISNe than SNe II, in spite of the fact that PISNe have the thicker hydrogen envelopes. This reason is that the gas velocities ($\sim 2000\text{--}3000 \text{ km s}^{-1}$) at the outermost He core for PISNe with the explosion energies higher than 10^{52} erg are a few times higher than those for SNe II. For $n_{\text{H},0} = 0.1\text{--}10 \text{ cm}^{-3}$, the collision times are $\simeq 10^3\text{--}10^4$ yr and decrease with increasing the ambient gas density. Note that this result is not consistent with the observations of the Cas

A SNR, where thermal emission from dust heated by the reverse shock has already detected at $\simeq 330$ yr after the explosion (Ennis et al. 2006 and references therein). This is because the progenitor of the Cas A is believed to have lost the considerable hydrogen envelope during their evolution (Young et al. 2006), in contrast to the Population III SNe considered in this paper. We shall discuss the effect of the hydrogen envelope on the evolution of dust in the SNR in § 4.

The fates of dust grains within SNRs heavily depend on their initial sizes a_{ini} as well as the chemical composition reflecting the difference in the sputtering yield and bulk density, as shown in Figure 3. For the standard model, the relatively small grains with $a_{\text{ini}} = 0.01 \mu\text{m}$ are efficiently decelerated due to the gas drag and are fully trapped into the hot plasma to be completely destroyed by the thermal sputtering. Note that the gas drag on grains with small radii is more efficient than that on larger grains, because the deceleration rate of grain is inversely proportional to its size (NKH06). Actually, the grains with the initial sizes less than $0.05 \mu\text{m}$ are trapped into the hot gas between the forward and reverse shocks and continue to be eroded by the thermal sputtering even at over 10^5 yr until they are completely destroyed. Larger grains of $a_{\text{ini}} = 0.1 \mu\text{m}$ undergo the kinetic and thermal sputtering while streaming in the hot gas. Thanks to the high bulk density, Fe grains with $a_{\text{ini}} = 0.1 \mu\text{m}$ are injected into the ISM, reducing the size by 52 %. On the other hand, C and Mg_2SiO_4 grains with $a_{\text{ini}} = 0.1 \mu\text{m}$ are trapped and eroded by the thermal sputtering in the denser region behind the forward shock, and their surface layers whose thicknesses are 43 and 69 % of their initial sizes are eroded, respectively, until 2×10^5 yr when the SNR enters into the radiative phase and the dense SN shell is formed behind the forward shock. These dust grains remain in the dense shell without further processing because the gas cools down quickly below 10^6 K. Thus, the decrease of sizes of these grains is truncated at a given size, and the erosion of dust with $a_{\text{ini}} = 0.05\text{--}0.2 \mu\text{m}$ results in the final size of $0.001\text{--}0.1 \mu\text{m}$, depending on their initial sizes. For $1 \mu\text{m}$ -sized C, Mg_2SiO_4 , and Fe grains, the kinetic sputtering reduces their sizes by 0.7, 6, and 8 %, respectively. Note that large grains with $a_{\text{ini}} \gtrsim 0.2 \mu\text{m}$ can go across even the forward shock and be injected into the ISM, because the deceleration due to the gas drag is very inefficient.

We should mention here that the degree of the erosion of dust is a complex function of the initial position and initial size of the dust as well as the sputtering yield. Fe grains formed in the innermost He core and travelling through the oxygen-rich gas undergo the efficient erosion, since the sputtering yield by an oxygen ion is ~ 50 times larger than that by a proton. In contrast, the degree of the erosion of C grains in the outermost He core is relatively small because they can quickly escape from the He core after the collision with the reverse shock and also have the sputtering yield lower than those of other dust species. Furthermore, without being decelerated efficiently, the larger grains with the high velocities

relative to gas are more efficiently eroded by sputtering in the relatively dense region near the forward shock front. However, the grains with the sizes larger than a given size can evade the erosion in the shocked hot gas within SNRs and are expelled into the ISM.

Although the processing of dust in the ISM is not the main subject of this paper, here we shall simply show the processing of dust injected into the ISM as a consequence of dust evolution in SNRs. Dust grains injected into the ISM can be consumed through the kinetic sputtering because of the difference in velocity between the ambient cool gas and the dust grains, while the grains can be also decelerated by the direct collisions with the gas. In this case, the ratio of the final radius a_{fin} to the initial size a_{ini} of dust is dependent only on the escape velocity w_0 defined as the velocity with which dust is injected into the ISM passing through the forward shock, and is given by

$$\frac{a_{\text{fin}}}{a_{\text{ini}}} = \exp \left[- \left(\frac{2m_{\text{sp}}}{3\mu_g} \right) \int_{w_f}^{w_0} \sum_i A_i Y_i^0(w) \frac{dw}{w} \right], \quad (1)$$

where m_{sp} is the average atomic mass of the elements sputtered from the grain, μ_g is the mean molecular weight of the gas, and $Y_i^0(w)$ is the sputtering yield at normal incidence by gas species i whose number abundance is A_i .

Figure 5 shows the results calculated by Equation (1) for the primordial gas composition as a function of the escape velocity. In the calculations, the final relative velocity w_{fin} is taken as 10 km s^{-1} , which is small enough for dust grains not to be eroded by the kinetic sputtering. Also we assume that the escape velocity equals to the initial velocity inside the He core, since very large grains are ejected to the ISM with high velocities, not being decelerated efficiently. Hence, the calculated a_{fin} gives the lower limit of the final size realized in the ISM. The final size acquired by each dust species is different, depending on the sputtering yield Y_i^0 and the average atomic mass m_{sp} , and decreases with increasing the escape velocity. The ratio of the final size to the initial size is $\simeq 0.8$ for C grains with $w_0 \sim 1300 \text{ km s}^{-1}$, $\simeq 0.5$ for Mg_2SiO_4 grains with $w_0 \sim 900 \text{ km s}^{-1}$, and $\simeq 0.5$ for Fe grains with $w_0 \sim 400 \text{ km s}^{-1}$. Thus, the sizes of very large grains supplied from SNe are decreased to 0.5–0.8 times those at the time of the ejection, but are not completely destroyed in the ISM. For PISNe with the explosion energies higher than 10^{52} erg , the sizes of Fe grains with the initial velocities of $\simeq 1000 \text{ km s}^{-1}$ decrease by 70 % in the ISM, although the sizes of C and Mg_2SiO_4 grains whose initial velocities are in the range of 2000–3000 km s^{-1} are not significantly different from those calculated for the standard model. Note that dust grains in the ISM are also processed by the high-velocity interstellar shocks driven by the ambient SNe (NKH06), which is the major mechanism of the dust destruction in the ISM.

3.3. *Efficiency of Dust Destruction*

The results described in § 3.2 imply that the size distribution of survived dust is greatly deficient in small-sized grains, compared with that at the time of dust formation. In Figure 6, we present the initial size distribution at the time of dust formation (Fig. 6a) and the size distribution of dust at the truncation time (Fig. 6b) for the standard model. The comparison of these figures clearly indicates that grains with the radii below a few tens Å are missing for almost all dust species. In particular, Al_2O_3 grains are completely destroyed because their initial sizes are smaller than $0.02 \mu\text{m}$. We can also see that the sizes of the relatively large grains are shifted to small sizes due to the erosion by sputtering. It should be pointed out here that the size distribution of survived dust is different from that by Bianchi & Schneider (2007): They have found that the final size distribution show a flattening towards smaller sizes without any abrupt truncation. The main reason of this difference is considered as follows. Bianchi & Schneider (2007) assumed that newly formed grains remain confined and trapped at their initial positions in the ejecta. Therefore, dust grains remaining at their initial positions cease to be eroded by sputtering on the timescale of $4\text{--}8 \times 10^4 \text{ yr}$ due to the decrease of the gas density caused by expansion. As shown in § 3.2, our results show that even small grains of $a_{\text{ini}} \leq 0.05 \mu\text{m}$ penetrate into the hot plasma between the forward and reverse shocks, and are trapped and completely destroyed in the hot gas with the relatively high density. On the other hand, the erosion of grains with the radii of $0.05\text{--}0.2 \mu\text{m}$ produces the grains with the final sizes of $0.001\text{--}0.1 \mu\text{m}$ remaining in the dense shell.

The critical size below which dust is destroyed is sensitive to the gas density in the ambient medium. Although the critical size weakly depends on the dust species and their initial positions, we can roughly estimate the average critical size for different gas density in the ISM. For $n_{\text{H},0} = 0.1 \text{ cm}^{-3}$, the upper limit of the initial size of dust completely destroyed is $\sim 0.01 \mu\text{m}$, and the lower limit of that ejected to the ISM is $\sim 0.03 \mu\text{m}$. For $n_{\text{H},0} = 10 \text{ cm}^{-3}$, the grains with $a_{\text{ini}} \lesssim 0.2 \mu\text{m}$ are destroyed, and the grains with $a_{\text{ini}} \gtrsim 0.5 \mu\text{m}$ are injected in the ISM. Note that the above critical sizes are true for the grain species except for C grains. The critical size of C grain is $0.006, 0.02, \text{ and } 0.07 \mu\text{m}$ for $n_{\text{H},0} = 0.1, 1, \text{ and } 10 \text{ cm}^{-3}$, respectively, and is a few times smaller than other dust species, because C grains are located at the outermost He core and also have the lower erosion rate by sputtering. Note that the initial sizes of Fe grains injected into the ISM are smaller than those of others by a factor of ~ 2 because of the high bulk density, and are $\gtrsim 0.02, 0.1, \text{ and } 0.25 \mu\text{m}$ for $n_{\text{H},0} = 0.1, 1, \text{ and } 10 \text{ cm}^{-3}$, respectively.

On the other hand, the critical size for each grain species is almost independent of the progenitor mass as long as the explosion energy of SN is the same, because the time evolution of temperature and density of gas within SNRs is similar. For PISNe with the

explosion energies higher than 10^{52} erg and more massive hydrogen envelopes, the critical size increases approximately by a factor of three, compared with that for SNe II. However, the initial size of dust ejected to the ISM is less than 2 times that for SNe II, because the high initial velocity inside the He core makes the dust grains easily escape from SNRs. These results lead to the conclusion that the large-sized grains dominate the mass of dust injected from SNe into the ISM.

Tables 1 and 2 summarize the mass fraction of dust destroyed ϵ_{dest} , piled up in the dense shell ϵ_{shell} , and ejected to the ISM ϵ_{eject} for the unmixed and mixed grain models, respectively. In Figures 7a and 7b, we also present the total mass of survived dust for both grain models, respectively, along with their initial total mass. We can first see that the mass of dust destroyed increases with increasing the surrounding gas density. In particular, for $n_{\text{H},0} = 10 \text{ cm}^{-3}$, all or almost all ($\gtrsim 85\%$) of dust grains formed in the ejecta are destroyed, and the mass of survived dust is less than $0.1 M_{\odot}$ for all models considered in this paper. This reason is as follows; the erosion of dust takes place in the hot gas between the forward and reverse shocks, whose density increases with the ambient gas density. Therefore, the higher ISM gas density leads to the efficient erosion and deceleration of dust through the more frequent collisions with the hot gas. Next, we find that the mass fraction of dust destroyed is generally higher for the mixed grain model than the unmixed grain model; for SNe II with $n_{\text{H},0} = 1 (0.1) \text{ cm}^{-3}$, $\epsilon_{\text{dest}} = 0.5\text{--}0.8 (0.2\text{--}0.4)$ for the unmixed grain model, while $\epsilon_{\text{dest}} = 0.9\text{--}0.99 (0.57\text{--}0.78)$ for the mixed grain model. This reflects the fact that the mixed grain model lacks the grains larger than $0.05 (0.01) \mu\text{m}$ in comparison with the unmixed grain model. Finally, it can be seen that dust grains formed in PISNe are more efficiently destroyed than those in SNe II, since the newly formed dust grains are dominated by the small-sized grains and the critical size is much larger. Thus, for $n_{\text{H},0} = 1 \text{ cm}^{-3}$, the mass of dust survived in PISNe is $0.1\text{--}1 M_{\odot}$ for both grain models and is almost the same as that ($0.07\text{--}0.5 M_{\odot}$) in the SNe II, though the mass of dust formed in PISNe is a few tens times higher than that in SNe II. Note that the dust destruction by reverse shocks is more effective than that by high-velocity interstellar shocks for the dust grains with the same size distribution (NKH06).

The destruction efficiency defined as the ratio of the mass of dust destroyed to the initial dust mass is given in Tables 3 and 4 for each dust species in the unmixed and mixed grain model, respectively. As mentioned above, the efficiency of dust destruction is greatly influenced by what fraction of the initial dust mass is occupied by the sizes larger than the critical size. Thus, the destruction efficiency for a given dust species is very sensitive to the initial size distribution. Note that it is difficult to find the clear dependence of the destruction efficiency of each dust species on the progenitor mass because the size distribution of dust at the time of dust formation is different from model to model. However, for example,

the efficiency of destruction of Al_2O_3 grain with $a_{\text{ini}} \lesssim 0.02 \mu\text{m}$ is ~ 1 for almost all cases considered in this paper. For the unmixed grain model, FeS and MgSiO_3 grains are also predominantly destroyed. On the other hand, Fe, Si, and C grains for which most of the mass is locked into the grains larger than $0.05 \mu\text{m}$ have the relatively small destruction efficiencies. For the mixed grain model, SiO_2 grains are the main dust species that are left in SNRs and/or are injected into the ISM. Therefore, we conclude that the chemical composition, size distribution, and amount of dust grains supplied from SNe to the ISM are quite different from those at the time of dust formation.

Here we shall discuss the dependence of the metallicity on the present results of calculations. First, it should be pointed out that the species of dust formed in the ejecta of SNe II and their size distributions are not sensitive to the metallicity of progenitor stars (Todini & Ferrara 2001; Nozawa 2003). Also the cooling function of gas for $Z \leq 10^{-3} Z_{\odot}$ is independent of the metallicity (Sutherland & Dopita 1993). Thus, the results of calculations presented in this paper can be directly applied to the evolution of dust in the ejecta of SNe II expanding into the ambient medium whose metallicity is less than $10^{-3} Z_{\odot}$. The increase of the metallicity in the ambient medium to the solar value greatly enhances the cooling of gas behind the forward shock and causes the time of the transition from nonradiative phase to radiative phase to be reduced to less than half of that for the zero-metallicity case. Nevertheless, the destruction efficiency of each grain species for $Z = Z_{\odot}$ decreases at most by 15 % of that for $Z = 0$. Therefore, the results of present study could be useful for evaluating the dust evolution in SNRs generated from SNe II, regardless of the initial metallicity of progenitor stars and ambient medium. However, as is demonstrated in the next section, the thickness of hydrogen envelope strongly affects the motion and destruction of dust within SNRs.

4. THE EFFECT OF THE HYDROGEN ENVELOPE ON THE EVOLUTION OF DUST IN SNR

As mentioned in § 3.2, for the SNe with the thick hydrogen envelopes, it takes at least more than 1000 yr for the reverse shocks to collide with the dust condensed inside the He core. On the other hand, the infrared observations of the Cas A SNR (Dwek et al. 1987; Lagage et al. 1996; Arendt et al. 1999; Douvion et al. 2001; Hines et al. 2004; Ennis et al. 2006) have revealed the thermal emission from warm dust formed in the ejecta at $\simeq 330$ yr after the explosion. This difference of the time at which dust grains inside the He core are swept up by the reverse shocks is attribute to the difference in the thickness of the hydrogen envelope of SNe. Therefore, in this section, we investigate the effect of the hydrogen envelope

on the evolution of dust in the SNR.

In order to illustrate the evolution of dust in the SNR generated from the SN whose hydrogen envelope is very thin, we adopt the model of ejecta with $M_{\text{pr}} = 20 M_{\odot}$ from Umeda & Nomoto (2002) and modify it by artificially reducing the mass of the hydrogen envelope from $13 M_{\odot}$ to $0.7 M_{\odot}$ at the time of explosion. Keeping the structure of the density, we simply scale up the gas velocity so that the explosion energy can equal to 10^{51} erg. We also assume the dust inside the He core is the same as that formed in primordial SN II with $M_{\text{pr}} = 20 M_{\odot}$.

Figure 8 illustrates the trajectories (Fig. 8a) and time evolutions of sizes (Fig. 8b) of C, Mg_2SiO_4 , and Fe grains with $a_{\text{ini}} = 0.01$ and $0.1 \mu\text{m}$ in the SNR calculated for $n_{\text{H},0} = 1 \text{ cm}^{-3}$. As can be expected, because the hydrogen envelope is very thin and the initial velocities of dust grains are very high (2000–5000 km s^{-1} depending on their initial positions), the dust grains inside the He core collide with the reverse shock at much earlier time; 120 yr for C grains, 570 yr for Mg_2SiO_4 grains, and 1300 yr for Fe grains. Contrary to SNe II with the thick hydrogen envelopes, even the grains with $a_{\text{ini}} = 0.1 \mu\text{m}$ can be ejected to the ISM without decreasing their sizes significantly; C and Mg_2SiO_4 grains with $a_{\text{ini}} = 0.1 \mu\text{m}$ reduce their sizes only by less than 6 %, while the sizes of Fe grains with $a_{\text{ini}} = 0.1 \mu\text{m}$ decrease by 18 % because the time staying in the hot gas is long, compared with C and Mg_2SiO_4 grains. The grains with $a_{\text{ini}} = 0.01 \mu\text{m}$ are trapped into the hot gas and are completely destroyed. In this case, the critical size below which dust is completely destroyed is $\sim 0.04 \mu\text{m}$, and the lower limit of the initial size of dust supplied to the ISM is $\sim 0.04 \mu\text{m}$ which is five times smaller than that for a SN II. Therefore, the thin hydrogen envelope as well as the high initial velocity of dust causes almost all survived dust grains to be injected into the ISM without being trapped into the gas within the SNR. The mass fraction of dust destroyed is 0.38, which is lower than 0.75 for the standard model, and thus more dust grains are supplied to the ISM. The result of calculation shows that the fates of dust grains formed in the ejecta strongly depend on the thickness of the hydrogen envelope.

However, we adopt the model of dust formed in a SN II and also consider the uniform ambient medium. The significant mass loss of massive stars during their evolution results in the circumstellar medium that is not uniform and homogeneous. In addition, the time evolution of the temperature and density of gas in the ejecta of SNe without the hydrogen envelopes such as Type Ib/c SNe is expected to be different from that in SNe II, which influences the dust formation in the ejecta. Therefore, we must clarify the size distribution and amount of dust grains formed in the ejecta to investigate the dependence of the evolution of dust on the type of SNe. This subject will be reported in the forthcoming paper.

5. *ELEMENTAL ABUNDANCES OF THE SECOND-GENERATION STARS*

Some extremely metal-poor (EMP) stars with $[\text{Fe}/\text{H}] \lesssim -2.5$ discovered in the Galactic halo have peculiar abundance patterns showing the modest or large (1–100 times) enhancements of C, N, O, Mg, and Si relative to solar (Venkatesan et al. 2006 and references therein). In particular, two hyper metal-poor (HMP) stars with $[\text{Fe}/\text{H}] \lesssim -5$, HE 0107-5240 ($[\text{Fe}/\text{H}] = -5.2$, Christlieb et al. 2002) and HE 1327-2326 ($[\text{Fe}/\text{H}] = -5.4$, Frebel et al. 2005) show extreme ($\gtrsim 10^2$ times) overabundances of C, N, and O relative to iron. Because the elemental composition of HMP stars expected to be the very early generation may strongly reflect the nucleosynthesis in Population III stars, several scenarios have been proposed to explain the origin of elemental abundances in low-mass HMP stars; the mixing fall-back in a core-collapse SN (Umeda & Nomoto 2005; Iwamoto et al. 2005), the nucleosynthesis and mass transfer in a first-generation binary star (Suda et al. 2004; Komiya et al. 2006), the pollution by the gas with heavy elements in the ISM (Shigeyama et al. 2003), and the combinations of these scenarios described above (Christlieb et al. 2004).

Recently, Venkatesan et al. (2006) have proposed that EMP stars are the second-generation stars formed in the dense shell of primordial SNRs and their peculiar abundances can be reproduced by the segregated transport of newly formed dust decoupled from the metal-rich gas in SNe. Adopting the dust models by Todini & Ferrara (2001) and Schneider et al. (2004), they calculated the sputtering and the transport of dust driven by the UV radiation field from the stellar cluster within a SNR. They have conclude that the progenitor mass range of 10–150 M_{\odot} qualitatively explains the enhancement of the elements composing dust grains (C, O, Mg, and Si) in EMP stars, though they did not compare their results with the abundance data on these metal-poor stars.

The results of the transportation and destruction of dust given in § 3.2 show that all dust grains remaining in primordial SNRs without being completely destroyed by sputtering can be accumulated in the dense SN shell at $\sim 10^5$ – 10^6 yr after the explosion. Thus, it is considered that the formation of the second-generation stars with solar mass scales could be possible in the shell contaminated with dust grains, as is investigated by Schneider et al. (2006). In this case, we can expect that the elemental compositions of dust grains piled up into the dense shell reflect the metal abundance patterns of the second-generation stars.

The iron-bearing dust species including the most important element Fe are Fe and FeS grains for the unmixed grain model, and Fe_3O_4 grain for the mixed grain model. Note that C grains cannot be formed in the mixed ejecta because the ejecta is oxygen-rich, and Fe_3O_4 grains with $a_{\text{ini}} \lesssim 0.05 \mu\text{m}$ are dominantly destroyed in the postshock flow and are rarely accumulated in the SN shell for $n_{\text{H},0} = 1$ and 10 cm^{-3} . Hence, we show only the results

calculated for the unmixed grain model. In addition, Fe and FeS grains are not significantly piled up in the shell of PISN remnants, since most of them are completely destroyed or are injected into the ISM. Thus, we focus on the results for Type II SNRs.

The abundances of C, O, Mg, and Si relative to Fe in the dense shell are summarized in Tables 5, where we neglect the contribution of metal atoms sputtered from the grains crossing the dense shell because the largest-sized grains are only eroded by less than 1% of their radii. The hydrogen mass in the dense SN shell $M_{\text{shell}}^{\text{H}}$ at the truncation time is given in Table 1. It can be seen from Table 5 that all models considered here predict the value of $[\text{Fe}/\text{H}]$ less than -4 , and most of them exhibit the value of $[\text{Fe}/\text{H}]$ ranging from -6 to -5 . Thus, two HMP stars are considered to be formed in the dense shell of primordial SNRs. Among the 9 models with $-6 \leq [\text{Fe}/\text{H}] \leq -5$, the abundances of Mg and Si are in the range of $-1.2 \leq [\text{Mg}/\text{Fe}] \leq 1.2$ and $-0.6 \leq [\text{Si}/\text{Fe}] \leq 2.7$, respectively, and 8 models can produce the overabundances of Mg and/or Si. This result suggests that the dust formed in the unmixed ejecta of SNe II can be responsible for the peculiar abundance patterns of Mg and Si in HMP stars. Although a few models ($20 M_{\odot}$ and $30 M_{\odot}$ for $n_{\text{H},0} = 1 \text{ cm}^{-3}$ and $25 M_{\odot}$ for $n_{\text{H},0} = 0.1 \text{ cm}^{-3}$) result in the overabundances of C and O as well as Mg and Si, $[\text{C}/\text{Fe}]$ and $[\text{O}/\text{Fe}]$ are limited to <1.6 and <0.6 , respectively.

For comparison, we apply the present calculations to the models of dust formation in the SN II with $M_{\text{pr}} = 22 M_{\odot}$ by Todini & Ferrara (2001) and in PISN with $M_{\text{pr}} = 195 M_{\odot}$ by Schneider et al. (2004). Because the sizes of the dust grains calculated by them are considerably small ($\lesssim 0.04 \mu\text{m}$) except for C grain, the grain species that can survive the destruction through the collisions with the reverse shocks is only C grain for the ambient gas density of $n_{\text{H},0} = 0.1\text{--}10 \text{ cm}^{-3}$. Thus, their dust models cannot explain the abundance patterns of the metals except for C observed in HMP and EMP stars.

6. SUMMARY

We investigate the evolution of dust formed at Population III SN explosions through the collision with the reverse shocks within SNRs. We adopt the models of dust grains obtained from the calculation of dust formation in Population III SNe by Nozawa et al. (2003) and take into account their spatial distribution and size distribution as the initial condition. The calculations carefully treat the dynamics, erosion, and heating of dust grains, and the evolution of temperature and density of gas in spherically symmetric shocks is solved as a function of time. We also discuss the effect of the hydrogen envelope on the evolution of dust in the SNR. Furthermore, from the analysis of the transport and destruction of dust within SNRs, we investigate the abundances of elements related to dust in the second-generation

stars formed in the dense shell of primordial SNRs.

The our main results are summarized as follows.

1. The time that the reverse shock encounters the dust that condensed inside the He core depends on the thickness of the H-envelope that was retained by the progenitors of the Population III SNe. If the progenitor stars did not undergo significant mass loss, the reverse shock will encounter the dust $\simeq 10^3$ – 10^4 yr after the explosion, depending on the density of gas in the ISM.

2. Once dust grains inside the He core collide with the reverse shocks, they will follow different trajectories depending on their initial sizes, resulting in the differential transport and destruction of dust in SNRs. For Type II SNRs expanding into the ISM with the density of $n_{\text{H},0} = 1 \text{ cm}^{-3}$, small grains with $a_{\text{ini}} \lesssim 0.05 \text{ }\mu\text{m}$ are rapidly trapped into the postshock flow and are completely destroyed by sputtering. Grains with $a_{\text{ini}} = 0.05$ – $0.2 \text{ }\mu\text{m}$ are trapped and remain in the dense shell behind the forward shock. Very large grains with $a_{\text{ini}} \gtrsim 0.2 \text{ }\mu\text{m}$ are ejected to the ISM through the forward shock without significantly decreasing their sizes.

3. The critical size below which dust is completely destroyed in SNRs is sensitive to the gas density in the ambient medium, and spans the range of 0.01 – $0.2 \text{ }\mu\text{m}$ for $n_{\text{H},0} = 0.1$ – 10 cm^{-3} . The resulting size distribution of survived dust is greatly deficient in small-sized grains, compared with that at the time of dust formation, although the erosion of large grains produces the smaller-sized grains. Thus, the mass of dust injected from SNe into the ISM is dominated by the large grains.

4. The total mass fraction of dust destroyed in SNRs ranges from 0.2 to 1 and increases with increasing the ambient gas density and explosion energy of SNe. The destruction efficiency of each dust species is very sensitive to the initial size distribution, and the dust species whose mass is predominantly occupied by the sizes larger than the critical size can survive. Therefore, the chemical composition, size distribution, and amount of dust grains supplied from SNe to the ISM are quite different from those at the time of dust formation.

5. The results for the evolution of dust in SNRs presented in this paper can be directly applied for the initial metallicity of progenitor stars and ambient medium less than $Z \leq 10^{-3} Z_{\odot}$, and could be useful for evaluating the evolution of dust in the Galactic SNRs generated from SNe II.

6. The fates of dust grains formed in the ejecta strongly depend on the thickness of the hydrogen envelope. For the SNR generated from the SN with the very thin hydrogen envelope, the collision time of the reverse shock with dust grains inside the He core is much

earlier. As long as the model of dust for SNe II is employed for the calculation, the mass of dust supplied to the ISM is larger than SNe II with the thick hydrogen envelopes.

7. If the elemental compositions of dust grains piled up in the SN shell reflect the metal abundance patterns of the second-generation stars formed in the dense shell of primordial SNRs, the dust formed in the unmixed ejecta of SNe II can be responsible for the peculiar abundance patterns of Mg and Si in HMP stars. However, another scenario could be necessary to produce the large overabundances of C and O observed in HMP stars.

The authors are grateful to the anonymous referee for critical comments that are useful for improving the manuscript. This work has been supported in part by a Grant-in-Aid for Scientific Research from the Japan Society for the Promotion of Sciences (16340051 and 18104003).

REFERENCES

- Arendt, R. G., Dwek, E., & Moseley, S. H. 1999, *ApJ*, 521, 234
- Baraffe, I., Heger, A., & Woosley, S. E. 2001. *ApJ*, 550, 890
- Beelen, A., Cox, P., Benford, D. J., Dowell, C. D., Kovacs, A., Bertoldi, F., Omont, A., & Carilli, C., L. 2006, *ApJ*, 642, 694
- Bertoldi, F., Carilli, C. L., Cox, P., Fan, X., Strauss, M. A., Beelen, A., Omont, A., & Zylka, R. 2003, *A&A*, 406, L55
- Bianchi, S., & Schneider, R. 2007, *MNRAS*, in press (astrp-ph/0704.0586)
- Bromm, V., Ferrara, A., Coppi, P. S., & Larson, R. B. 2001, *MNRAS*, 328, 969
- Cazaux, S., & Spaans, M. 2004, *ApJ*, 611, 40
- Christlieb, N., et al. 2002, *Nature*, 419, 904
- Christlieb, N., Gustafsson, B., Korn, A. J., Barklem, P. S., Beers, T. C., Bessell, M. S., Karlsson, T., & Mizuno-Wiedner, M. 2004, *ApJ*, 603, 708
- Douvion, T., Lagage, P. O., & Pantin, E. 2001, *A&A*, 369, 589
- Draine, B. T., & Salpeter, E. E. 1979, *ApJ*, 231, 77

- Dwek, E., Dinerstein, H. L., Gillett, F. C., Hauser, M. G., & Rice, W. L. 1987, *ApJ*, 315, 571
- Dwek, E., & Arendt, R. G. 1992, *ARA&A*, 30, 11
- Dwek, E., Galliano, F., & Jones, A. P. 2007, *ApJ*, in press
- Ennis, J. A., Rudnick, L., Reach, W. T., Smith, J. D., Rho, J., Delaney, T., Gomez, H., & Kozasa, T. 2006, *ApJ*, 652, 376
- Frebel, A., et al. 2005, *Nature*, 434, 871
- Hines, D. C., et al. 2004, *ApJS*, 154, 290
- Hines, D. C., Krause, O., Rieke, G. H., Fan, X., Blaylock, M., & Neugebauer, G. 2006, *ApJ*, 641, L85
- Hirashita, H., & Ferrara, A. 2002, *MNRAS*, 337, 921
- Hirashita, H., Nozawa, T., Kozasa, T., Ishii, T. T., & Takeuchi, T. T. 2005, *MNRAS*, 357, 1077
- Iwamoto, N., Umeda, H., Tominaga, N., Nomoto, K., & Maeda, K. 2005, *Science*, 309, 451
- Kitayama, T., Yoshida, N., Susa, H., & Umemura, M. 2004, *ApJ*, 613, 631
- Komiya, Y., Suda, T., Minaguchi, H., Shigeyama, T., Aoki, Y., & Fujimoto, M. Y. 2007, *ApJ*, in press (astro-ph/0610670)
- Kozasa, T., Hasegawa, H., & Nomoto, K. 1989, *ApJ*, 344, 325
- Lagage, P. O., Claret, A., Ballet, J., Boulanger, F., Cesarsky, C. J., Cesarsky, D., Fransson, C., & Pollock, A. 1996, *A&A*, 315, L273
- Machida, M. N., Tomisaka, K., Nakamura, F., & Fujimoto, M. Y. 2005, *ApJ*, 622, 39
- Maiolino, R., Oliva, E., Ghinassi, F., Pedani, M., Mannucci, F., Mujica, R., & Juarez, Y. 2004a, *A&A*, 420, 889
- Maiolino, R., Schneider, R., Oliva, E., Bianchi, S., Ferrara, A., Mannucci, F., Pedani, M., & Roca Sogorb, M. 2004b, *Nature*, 431, 533
- Mair, G., Müllar, E., Hillebrandt, W., & Arnold, C. N. 1988, *A&A*, 199, 114
- McKee, C. F., Hollenbach, D. J., Seab, C. G., & Tielens, A. G. G. M. 1987, *ApJ*, 318, 674

- Morgan, H. L., & Edmunds, M. G. 2003, MNRAS, 343, 427
- Nozawa, T., Kozasa, T., & Habe, A. 2006, ApJ, 648, 435
- Nozawa, T., 2003, Master Thesis, Hokkaido University
- Nozawa, T., Kozasa, T., Umeda, H., Maeda, K., & Nomoto, K. 2003, ApJ, 598, 785
- Omukai, K., Tsuribe, T., Schneider, R., & Ferrara, A. 2005, ApJ, 626, 627
- Priddey, R. S., Isaak, K. G., McMahon, R. G., Robson, E. I., & Pearson, C. P. 2003, MNRAS, 344, L74
- Raymond, J. C., & Smith, B. W. 1977, ApJS, 35, 419
- Robson, I., Priddey, R. S., Isaak, K. G., & McMahon, R. G. 2004, MNRAS, 351, L29
- Schneider, R., Ferrara, A., & Salvaterra, R. 2004, MNRAS, 351, 1379
- Schneider, R., Omukai, K., Inoue, A. K., & Ferrara, A. 2006, MNRAS, 369, 1437
- Shigeyama, T., Tsujimoto, T., & Yoshii, Y. 2003, ApJ, 586, L57
- Smith, N., & Owocki, S. P. 2006, ApJ, 645, L45
- Smith, R. K., Brickhouse, N. S., Liedahl, D. A., & Raymond, J. C. 2001, ApJ, 556, L91
- Suda, T., Aikawa, M., Machida, M. N., Fujimoto, M. Y., & Iben Jr., I. 2004, ApJ, 611, 476
- Sutherland, R. S., & Dopita, M. A. 1993, ApJS, 88, 253
- Todini, P., & Ferrara, A. 2001, MNRAS, 325, 726
- Truelove, J. K., & McKee, C. F. 1999, ApJS, 120, 299
- Umeda, H., & Nomoto, K. 2002, ApJ, 565, 385
- Umeda, H., & Nomoto, K. 2005, ApJ, 619, 427
- van Albada, G. D., van Leer, B., & Roberts, W. W. Jr. 1982, A&A, 108, 76
- Venkatesan, A., Nath, B., B., & Shull, J. M. 2006, ApJ, 640, 31
- Young, P. A., Fryer, C. L., Hungerford, A., Arnett, D., Rockefeller, G., Timmes, F. X., Voit, B., Meakin, C., & Eriksen, K. 2006, ApJ, 640, 891

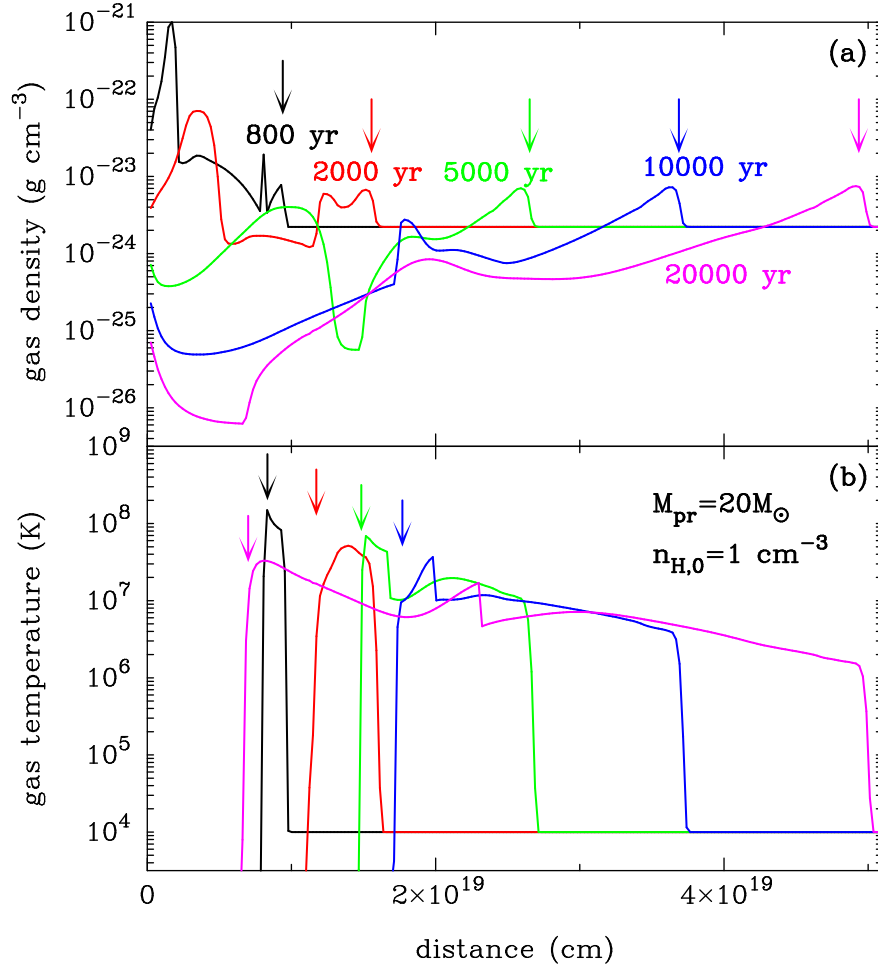


Fig. 1.— The structures of (a) the density and (b) the temperature of the gas at given times within the SNR generated from the explosion of star with $M_{\text{pr}} = 20 M_{\odot}$ and expanding into the ISM with $n_{\text{H},0} = 1 \text{ cm}^{-3}$ (the standard model). The positions of the forward and reverse shocks are indicated by the downward arrows in (a) and (b), respectively. *See the electronic edition of the Journal for a color version of this figure.*

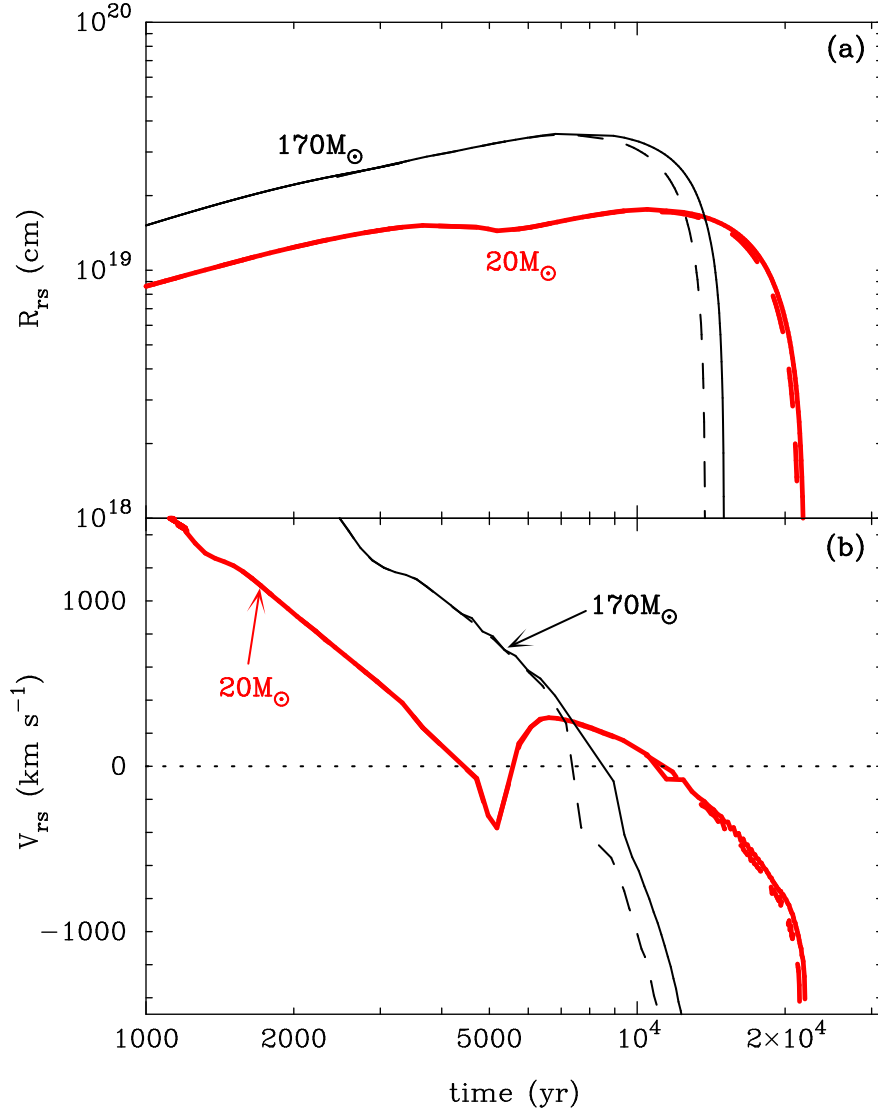


Fig. 2.— The time evolution of (a) the position R_{rs} and (b) the velocity V_{rs} of the reverse shock. The thick solid curves represents the results for the standard model with $M_{pr} = 20 M_{\odot}$ and $n_{H,0} = 1 \text{ cm}^{-3}$, and the thin solid curves for the model with $M_{pr} = 170 M_{\odot}$ and $n_{H,0} = 1 \text{ cm}^{-3}$. The results that do not include the cooling by thermal emission from dust are also shown by the thick and thin dashed curves for $M_{pr} = 20 M_{\odot}$ and $170 M_{\odot}$, respectively. See the electronic edition of the Journal for a color version of this figure.

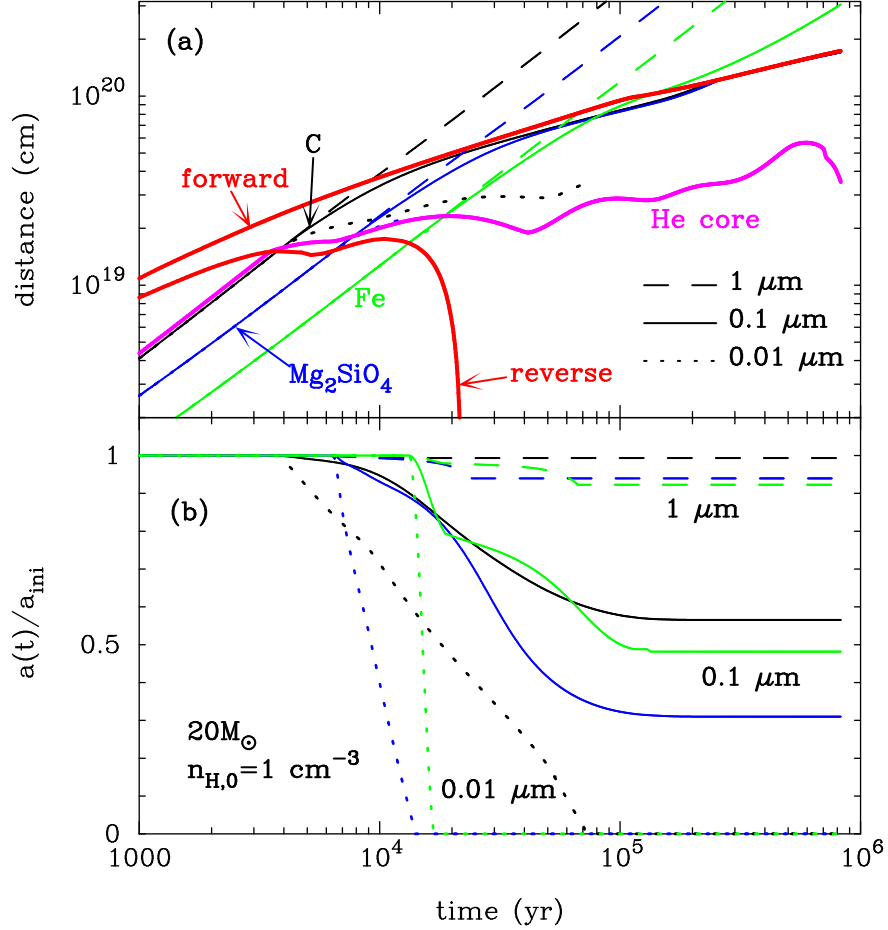


Fig. 3.— The time evolutions of (a) the positions and (b) the ratios of size to the initial size of dust grains within the SNR for the standard model. The positions of the forward and reverse shocks are depicted by the thick solid curves in (a), along with the position of the surface of the He core. Among nine dust species for the unmixed grain model, are shown C, Mg₂SiO₄, and Fe grains with the initial sizes of 0.01 μm (dotted lines), 0.1 μm (solid lines), and 1 μm (dashed lines), respectively. See the electronic edition of the Journal for a color version of this figure.

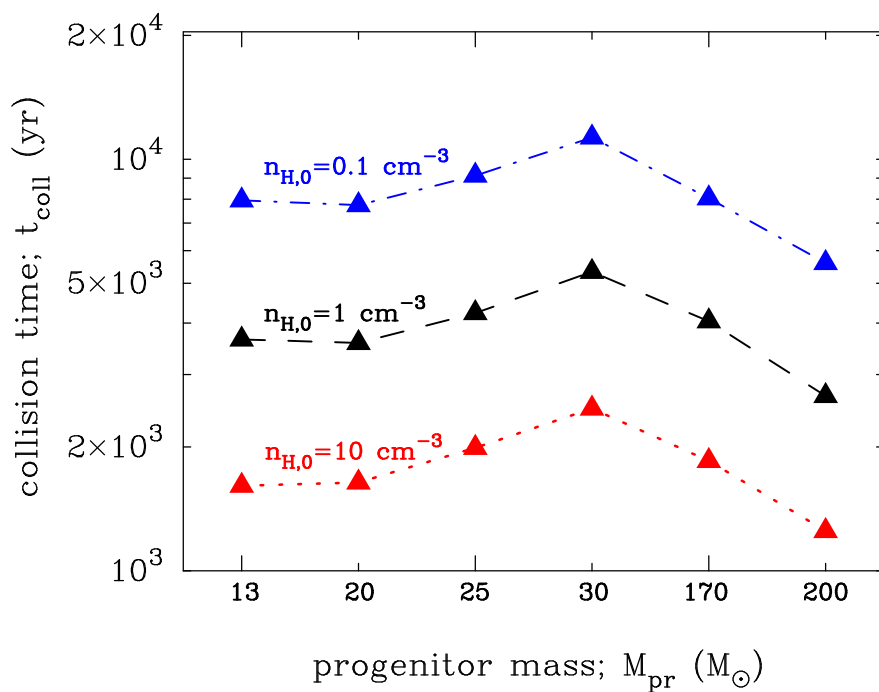


Fig. 4.— The collision time t_{coll} of the reverse shocks with the He core vs. the progenitor stellar mass for different gas density in the ISM. The results for $n_{\text{H},0} = 0.1, 1, \text{ and } 10 \text{ cm}^{-3}$ are connected by the dot-dashed, dashed, and dotted lines, respectively. *See the electronic edition of the Journal for a color version of this figure.*

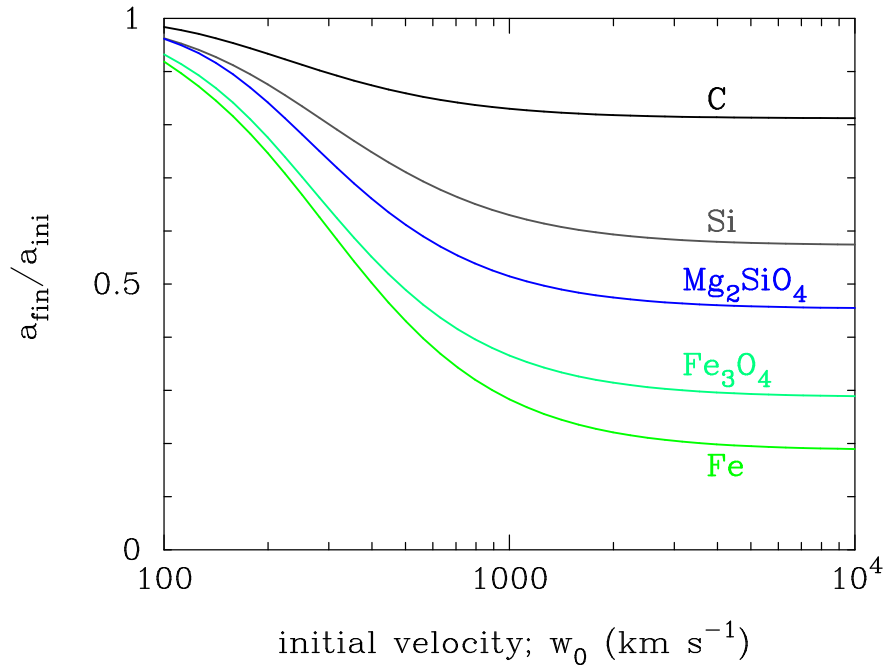


Fig. 5.— The ratio of the final size a_{fin} to the initial size a_{ini} of dust eroded by the kinetic sputtering in the ISM with the primordial gas composition as a function of the escape velocity w_0 , where the final relative velocity w_{fin} is taken as 10 km s^{-1} . The results are shown for C, Si, Mg_2SiO_4 , Fe_3O_4 , and Fe grains. *See the electronic edition of the Journal for a color version of this figure.*

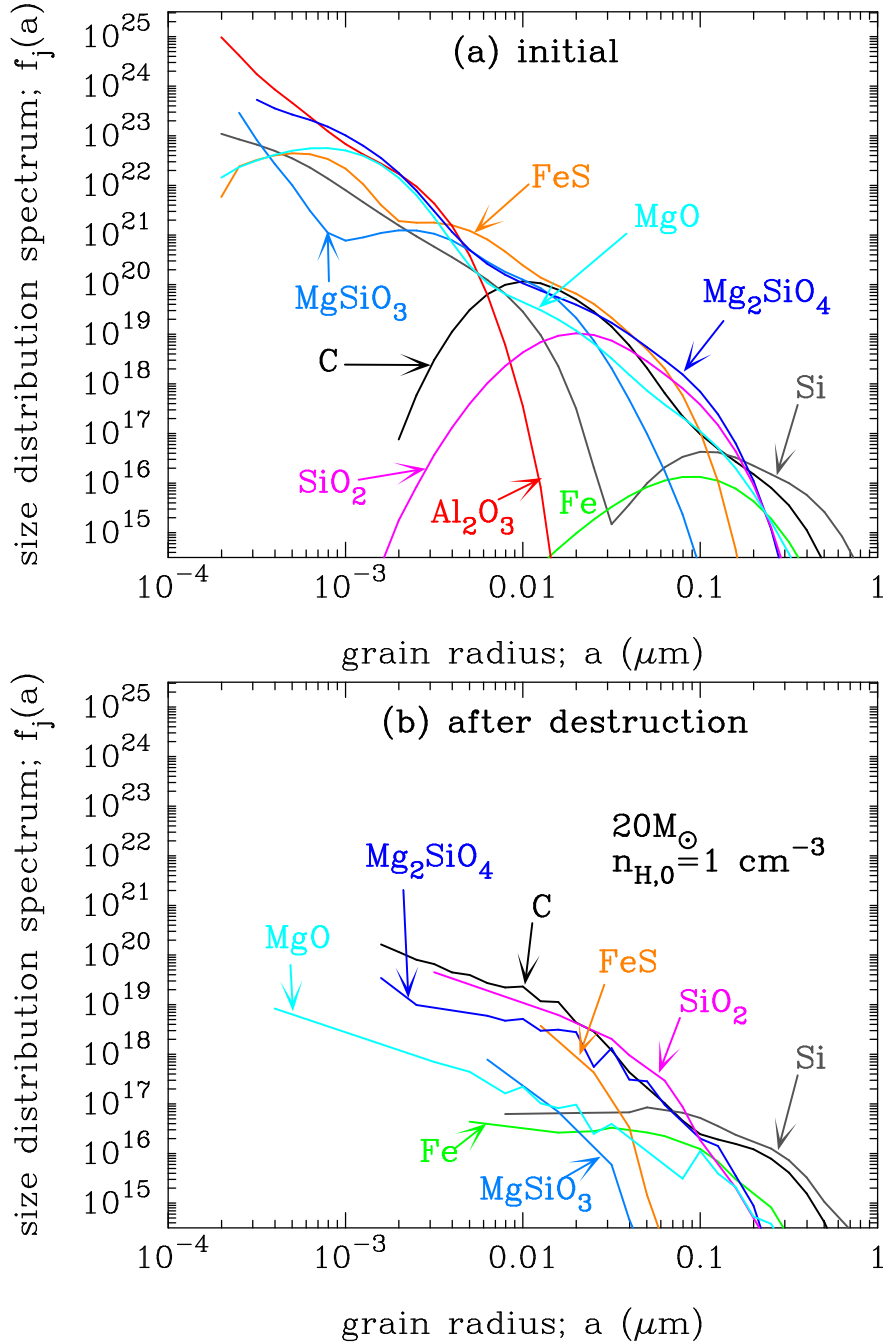


Fig. 6.— The size distribution of each dust species for the standard model; (a) for the initial size distribution before destruction and (b) for the resulting size distribution of survived dust after destruction. *See the electronic edition of the Journal for a color version of this figure.*

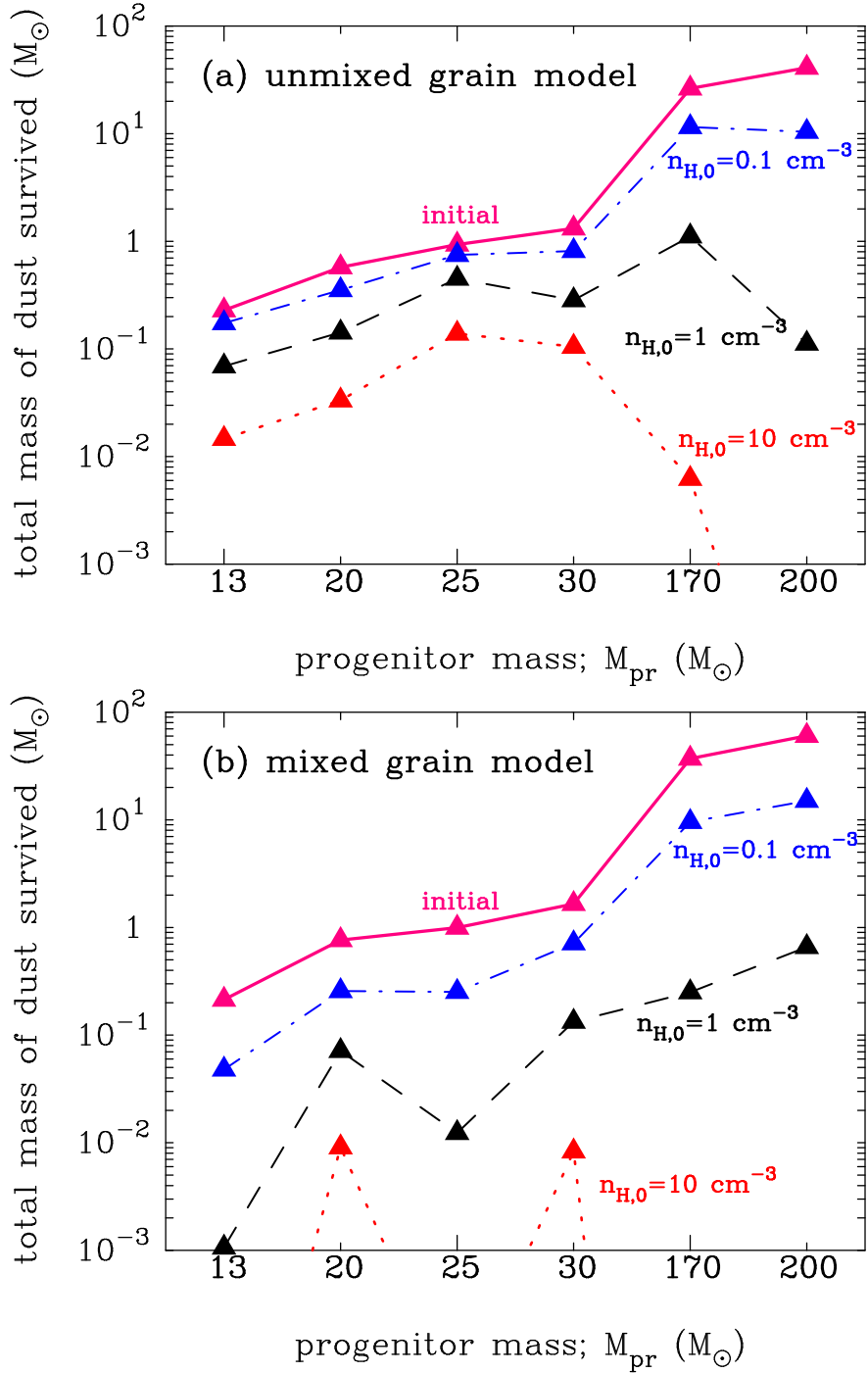


Fig. 7.— The total mass of survived dust for the various progenitor mass and the gas density in the ISM (a) for the unmixed grain model and (b) for the mixed grain model. The results for $n_{\text{H},0} = 0.1, 1, \text{ and } 10 \text{ cm}^{-3}$ are connected by the dot-dashed, dashed, and dotted lines, respectively. The solid lines are for the initial total mass of dust at the time of dust formation. *See the electronic edition of the Journal for a color version of this figure.*

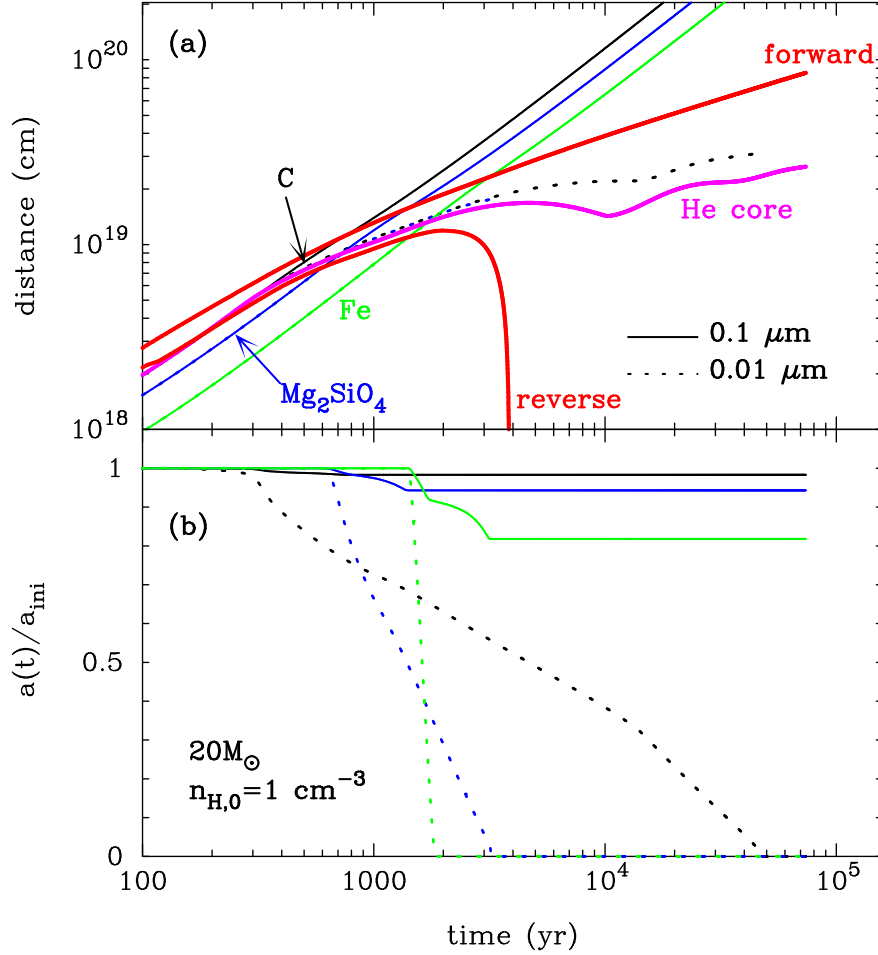


Fig. 8.— The time evolutions of (a) the positions and (b) the ratios of size to the initial size of dust grains within the SNR from the SN with the hydrogen envelope of $0.7 M_{\odot}$ and the explosion energy of 10^{51} erg for $n_{\text{H},0} = 1 \text{ cm}^{-3}$. The positions of the forward and reverse shocks are depicted by the thick solid curves in (a), along with the position of the surface of the He core. Among nine dust species for the unmixed grain model, are shown C, Mg_2SiO_4 , and Fe grains with the initial sizes of $0.01 \mu\text{m}$ (dotted lines) and $0.1 \mu\text{m}$ (solid lines), respectively. See the electronic edition of the *Journal* for a color version of this figure.

Table 1. THE MAIN RESULTS OF CALCULATIONS FOR THE UNMIXED GRAIN MODEL

M_{pr} (M_{\odot})	ϵ_{dest}	ϵ_{eject}	ϵ_{shell}	t_{tr} (10^6 yr)	$M_{\text{shell}}^{\text{H}}$ ($10^4 M_{\odot}$)
$n_{\text{H},0} = 0.1 \text{ cm}^{-3}$					
13	0.240	0.756	0.004	2.13	2.96
20	0.386	0.610	0.004	2.05	2.58
25	0.198	0.800	0.002	2.12	2.89
30	0.383	0.614	0.003	2.11	2.83
170	0.562	0.438	<0.001	4.58	34.4
200	0.746	0.247	0.007	5.13	50.2
$n_{\text{H},0} = 1 \text{ cm}^{-3}$					
13	0.698	0.256	0.046	0.814	2.07
20	0.752	0.231	0.017	0.767	1.72
25	0.517	0.474	0.009	0.800	1.97
30	0.785	0.206	0.009	0.790	1.88
170	0.958	0.040	0.002	1.81	25.4
200	0.997	0.002	0.001	2.02	35.2
$n_{\text{H},0} = 10 \text{ cm}^{-3}$					
13	0.936	0.004	0.060	0.308	1.31
20	0.942	0.013	0.045	0.301	1.21
25	0.851	0.103	0.046	0.310	1.33
30	0.920	0.042	0.038	0.309	1.31
170	0.999	<0.001	<0.001	0.723	18.0
200	1.00	<0.001	<0.001	0.825	27.1

Note. — For a given $n_{\text{H},0}$, the mass fraction of dust destroyed ϵ_{dest} , piled up in the dense shell ϵ_{shell} , and ejected to the ISM ϵ_{eject} as a function of the progenitor mass M_{pr} for the unmixed grain model. The truncation time t_{tr} and the hydrogen mass $M_{\text{shell}}^{\text{H}}$ in the dense SN shell are given

by the units of 10^6 yr and $10^4 M_{\odot}$, respectively

Table 2. THE MAIN RESULTS OF CALCULATIONS FOR THE MIXED GRAIN MODEL

M_{pr} (M_{\odot})	ϵ_{dest}	ϵ_{eject}	ϵ_{shell}	t_{tr} (10^6 yr)	$M_{\text{shell}}^{\text{H}}$ ($10^4 M_{\odot}$)
$n_{\text{H},0} = 0.1 \text{ cm}^{-3}$					
13	0.775	0.212	0.013	2.14	2.96
20	0.664	0.311	0.025	2.05	2.57
25	0.747	0.245	0.008	2.10	2.82
30	0.569	0.415	0.016	2.10	2.80
170	0.742	0.258	<0.001	4.55	33.7
200	0.751	0.248	0.001	5.12	49.8
$n_{\text{H},0} = 1 \text{ cm}^{-3}$					
13	0.995	0.001	0.004	0.814	2.07
20	0.907	0.075	0.018	0.767	1.71
25	0.988	0.009	0.003	0.800	1.95
30	0.920	0.060	0.020	0.788	1.86
170	0.993	0.007	<0.001	1.81	24.8
200	0.989	0.011	<0.001	2.00	34.2
$n_{\text{H},0} = 10 \text{ cm}^{-3}$					
13	1.00	0.	<0.001	0.309	1.33
20	0.988	0.002	0.010	0.301	1.21
25	1.00	0.	<0.001	0.316	1.38
30	0.995	<0.001	0.005	0.308	1.29
170	1.00	0.	<0.001	0.726	17.8
200	1.00	0.	0.	0.817	26.0

Note. — Same as Table 1, but for the mixed grain model.

Table 3. THE DESTRUCTION EFFICIENCY OF EACH DUST SPECIES FOR THE UNMIXED GRAIN MODEL

M_{pr} (M_{\odot})	Fe	Si	FeS	MgSiO ₃	SiO ₂	Al ₂ O ₃	Mg ₂ SiO ₄	MgO	C
$n_{\text{H},0} = 0.1 \text{ cm}^{-3}$									
13	0.209	0.257	0.939	0.892	0.297	1.00	0.349	0.615	0.048
20	0.210	0.127	0.881	0.945	0.518	1.00	0.437	0.440	0.146
25	0.089	0.061	0.693	0.570	0.086	0.999	0.201	0.520	0.080
30	0.099	0.077	0.636	0.901	0.277	0.992	0.543	0.412	0.299
170	0.644	0.273	1.00	0.987	0.441	1.00	0.776	0.772	0.284
200	0.712	0.787	1.00	0.990	0.438	1.00	0.865	0.820	0.210
$n_{\text{H},0} = 1 \text{ cm}^{-3}$									
13	0.715	0.660	1.00	0.998	0.882	1.00	0.964	0.997	0.520
20	0.661	0.493	0.999	0.999	0.926	1.00	0.961	0.925	0.447
25	0.379	0.289	0.984	0.968	0.369	1.00	0.719	0.934	0.284
30	0.405	0.349	0.970	0.997	0.745	1.00	0.989	0.946	0.842
170	0.999	0.872	1.00	1.00	0.998	1.00	1.00	1.00	0.985
200	0.989	0.999	1.00	1.00	0.992	1.00	1.00	1.00	0.996
$n_{\text{H},0} = 10 \text{ cm}^{-3}$									
13	0.958	0.894	1.00	1.00	0.995	1.00	1.00	1.00	0.893
20	0.961	0.851	1.00	1.00	1.00	1.00	1.00	1.00	0.896
25	0.861	0.699	1.00	1.00	1.00	1.00	0.998	1.00	0.727
30	0.824	0.706	1.00	1.00	0.958	1.00	1.00	1.00	0.990
170	1.00	0.999	1.00	1.00	1.00	1.00	1.00	1.00	1.00
P200	1.00	1.00	1.00	1.00	1.00	1.00	1.00	1.00	1.00

Note. — For a given $n_{\text{H},0}$, the mass fraction of dust destroyed as a function of the progenitor mass M_{pr} for each grain species in the unmixed grain model.

Table 4. THE DESTRUCTION EFFICIENCY OF EACH DUST SPECIES FOR THE MIXED GRAIN MODEL

M_{pr} (M_{\odot})	Al_2O_3	MgSiO_3	Mg_2SiO_4	SiO_2	Fe_3O_4
$n_{\text{H},0} = 0.1 \text{ cm}^{-3}$					
13	1.00	0.862	0.868	0.676	0.788
20	1.00	0.913	0.788	0.518	0.992
25	1.00	0.910	0.877	0.596	0.999
30	0.997	0.802	0.620	0.461	0.999
170	1.00	0.961	0.957	0.585	1.00
200	1.00	0.984	0.995	0.615	0.999
$n_{\text{H},0} = 1 \text{ cm}^{-3}$					
13	1.00	0.999	0.999	0.988	0.999
20	1.00	0.996	0.977	0.850	1.00
25	1.00	1.00	1.00	0.976	1.00
30	1.00	0.994	0.951	0.875	1.00
170	1.00	1.00	1.00	0.989	1.00
200	1.00	1.00	1.00	0.983	1.00
$n_{\text{H},0} = 10 \text{ cm}^{-3}$					
13	1.00	1.00	1.00	0.999	1.00
20	1.00	1.00	1.00	0.980	1.00
25	1.00	1.00	1.00	1.00	1.00
30	1.00	1.00	0.996	0.976	1.00
170	1.00	1.00	1.00	1.00	1.00
P200	1.00	1.00	1.00	1.00	1.00

Note. — Same as Table 3, but for each grain species in the mixed grain model.

Table 5. ELEMENTAL ABUNDANCES IN SN SHELL

M_{pr} (M_{\odot})	[Fe/H]	[C/Fe]	[O/Fe]	[Mg/Fe]	[Si/Fe]
$n_{\text{H},0} = 0.1 \text{ cm}^{-3}$					
13	−6.43	−0.274	−0.699	−0.230	1.92
20	−5.20	0.117	−0.595	0.034	0.410
25	−5.90	1.11	−1.42	−0.500	−0.552
30	−5.56	0.566	−0.043	0.739	0.866
$n_{\text{H},0} = 1 \text{ cm}^{-3}$					
13	−5.15	1.11	−0.555	−0.459	1.01
20	−5.53	0.992	0.585	1.16	1.87
25	−5.23	1.09	−0.412	0.407	0.989
30	−5.11	0.797	0.242	1.09	1.26
$n_{\text{H},0} = 10 \text{ cm}^{-3}$					
13	−4.13	0.284	−2.54	−3.89	0.599
20	−4.92	0.946	−2.15	−1.80	2.14
25	−5.10	1.60	0.122	0.232	2.34
30	−5.11	−0.207	0.375	−1.23	2.66

Note. — [Fe/H] and abundances of C, O, Mg, and Si relative to Fe in the shell of primordial Type II SNRs for given M_{pr} and $n_{\text{H},0}$ with the unmixed grain model.